Spin-noise-induced synchronization between non-overlapping laser beams

Shiming Song,[1,2] Min Jiang,[1,2] Yushu Qin,[1,2] Ze Wu,[1,2] Haowen Su,[1,2]
Ren-bao Liu,[3,4,5,6] Dieter Suter,[7] and Xinhua Peng[1,2,8,*]

[1]*CAS Key Laboratory of Microscale Magnetic Resonance and School of Physical Sciences, University of Science and Technology of China, Hefei 230026, China*
[2]*CAS Center for Excellence in Quantum Information and Quantum Physics, University of Science and Technology of China, Hefei 230026, China*
[3]*Department of Physics, The Chinese University of Hong Kong, Shatin, New Territories, Hong Kong, China*
[4]*Centre for Quantum Coherence, The Chinese University of Hong Kong, Shatin, New Territories, Hong Kong, China*
[5]*The Hong Kong Institute of Quantum Information Science and Technology, The Chinese University of Hong Kong, Shatin, New Territories, Hong Kong, China*
[6]*New Cornerstone Science Laboratory, The Chinese University of Hong Kong, Shatin, New Territories, Hong Kong, China*
[7]*Fakultät Physik, Technische Universität Dortmund, D-44221 Dortmund, Germany*
[8]*Hefei National Laboratory, University of Science and Technology of China, Hefei 230088, China*

(Received 19 March 2024; revised 18 July 2024; accepted 28 August 2024; published 10 September 2024)

Noise-induced synchronizations have led to diverse phenomena and applications. Here, we propose and demonstrate an approach towards inducing synchronizations between non-overlapping laser beams by intrinsic spin noise. Two linearly polarized and non-overlapping laser beams propagate through a vapor of flying unpolarized alkali atoms and capture their correlated noise properties by the atom-light interaction, resulting in synchronization between the two laser beams. Using correlation spectra, we demonstrate the nearly in phase synchronization at the atomic Larmor frequency between the two laser beams, which can easily be varied across a wide frequency range by the magnetic-field strength. Moreover, we show that the degree of synchronization increases with the atomic density, and the synchronization remains effective when the Larmor frequencies in the regions of the two laser beams are different. Our method may be useful for applications like secure key distribution and secure communication.

DOI: 10.1103/PhysRevA.110.033105

I. INTRODUCTION

Spatially separate systems can become synchronized in many different ways in physical [1,2], chemical [3], biological [4,5], and engineering systems [6]. Various mechanisms have been studied to induce synchronization, such as forced synchronization induced by external drives [7] and spontaneous synchronization induced by interactions [8]. Noise is inevitable in practical systems and is generally considered to have a negative impact on synchronization [9]. Nevertheless, recent studies indicated that noise can actually induce stable synchronization [4,10–14]. For instance, when applied to subsystems with similar response characteristics, common or correlated noise can lead to synchronized noisy behavior in initially independent subsystems [4,11,12]. Recently, noise-induced synchronization has attracted significant attention, with potential applications in the areas such as brain-inspired computing [14] and secure key distribution [11].

Spin noise in spin ensembles arises from the statistical nature of intrinsic random flips of individual spins and has been widely observed in spin systems, such as alkali atomic vapors [15–23], quantum dot ensembles [24], and semiconductor systems [25,26]. Currently, optical measurements of spin noise have emerged as a crucial way to numerous applications, such as the nonperturbative investigation of spin dynamics [15,16,19–28], the generation of quantum random numbers [18], and the quantification of spin squeezing [29].

Laser beams are often used to monitor spin noise through the rotation of the optical polarization by the spins. The coupling can be adjusted by spin and optical parameters [16]. If several laser beams interact with the same medium, they can acquire correlated noise properties from the interaction with the spin system, and their polarizations can be thus synchronized [30]. Moreover, multiple laser beams can acquire correlated noise properties from spin ensembles due to spin-spin interactions [21,31,32]. Up to now, experimental research has focused on the method of overlapping multiple laser beams.

Here, we use a different approach: The two laser beams propagate parallel through an atomic vapor cell, interacting with different atomic ensembles. However, the freely moving atoms can uniformly redistribute throughout the entire cell many times during the lifetime of their spin states. Recent theoretical studies suggest that, in such a scenario, the spin noise in these ensembles can become correlated [33–35], leading to closely correlated optical polarization modulation in both laser beams via atom-light interaction. The

*Contact author: xhpeng@ustc.edu.cn

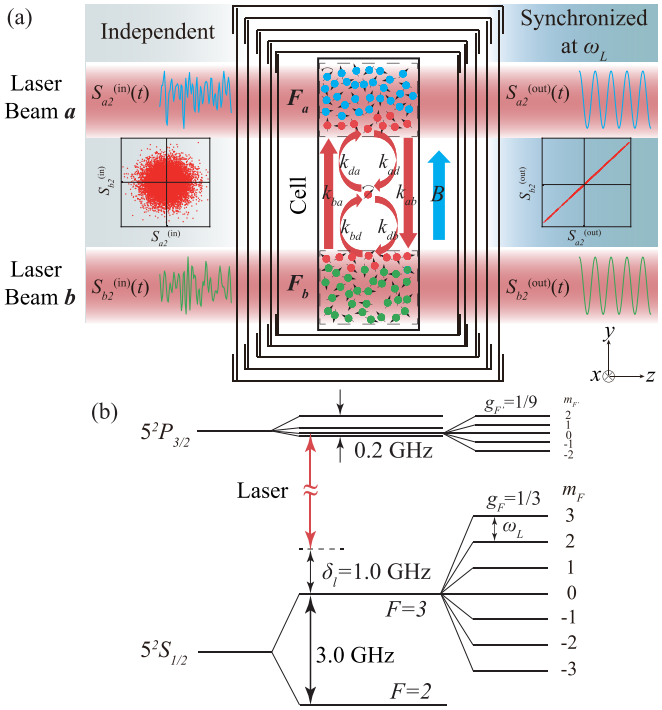

FIG. 1. Schematic of spin-noise-induced synchronization between non-overlapping laser beams. (a) Experimental setup and schematic correlation plots between Stokes components $S_2(t)$ for independent and perfectly synchronized laser beams. Two non-overlapping input laser beams a and b interact with the collective spins $\boldsymbol{F}_a$ and $\boldsymbol{F}_b$, respectively. Flying spins denoted by the red color travel between $\boldsymbol{F}_a$ and $\boldsymbol{F}_b$, imprinting their coherent spin dynamics onto the two laser beams. (b) Energy-level diagram of the ^{85}Rb atoms in the magnetic field $\boldsymbol{B}$.

synchronization between the polarization directions of two polarized laser beams is analyzed by the correlation spectra of two laser beams. We observe the nearly in phase synchronization between two laser beams at the atomic Larmor frequency. Furthermore, we investigate the synchronization with varying experimental conditions, including Larmor frequency, vapor temperature, and magnetic field gradient, and the experimental results align well with the theoretical predictions. As spin noise is intrinsically unpredictable [18], our technique produces synchronized random laser beams which have been extensively researched in the field of the secure key distribution [11].

This paper is organized as follows. In Sec. II, we introduce the model of the spin-noise-induced synchronization between two non-overlapping laser beams. In Sec. III, we present the theoretical results derived from the model and characterize the synchronization using the correlation spectra. Section IV presents the experimental results under different conditions. Finally, we present conclusions and discussion in Sec. V.

II. PHYSICAL MODEL

Figure 1(a) shows our experimental setup to synchronize two non-overlapping laser beams by the spin noise of a ^{85}Rb atomic ensemble encapsulated in a cell with no buffer gas [36]. The inner surfaces of the cell are coated with octadecyltrichlorosilane (OTS) to minimize the effect of wall collisions on the atomic spins, leading to a wall-relaxation rate on the order of tens of s^{-1} [22,37]. Two spatially separated laser beams propagate through the cell along the z direction. Their frequency is set at $\delta_l = 1$ GHz below the ^{85}Rb D_2 optical transition ($5S_{1/2} - 5P_{3/2}$; 780 nm), as shown in Fig. 1(b). This detuning is larger than the dominating Doppler broadening $\Delta_l \approx 500$ MHz of the optical absorption line to reduce the optical pumping of the spin ensemble to a rate of about 3.3 s^{-1} [see Eqs. (A18)–(A21) in the Appendix]. For spins in the $F = 2$ state, the detuning is much larger than for the $F = 3$ state [see Fig. 1(b)]. Accordingly, the atom-light coupling coefficient $G \propto 1/\delta_l$ is much stronger for spins in the $F = 3$ hyperfine level than that for those in $F = 2$; this allows us to focus only on the spins in $F = 3$. As discussed in more detail below, both laser beams are linearly polarized along the x direction before they enter the cell.

The dynamics of the atomic spins in a magnetic field $\boldsymbol{B} = (0, B, 0)$ can be described by the stochastic Bloch equation

$$d\boldsymbol{F} = (g_F \mu_B \boldsymbol{F} \times \boldsymbol{B} - \gamma \boldsymbol{F})dt + Q d\boldsymbol{W}, \tag{1}$$

where $\boldsymbol{F} = \sum_{j=1}^{N_{\rm at}} \boldsymbol{f}^j$ is the collective spin, with $\boldsymbol{f}^j$ being the angular momentum of the jth atom and $N_{\rm at}$ being the number of atoms in the $F = 3$ hyperfine level. g_F is the effective g factor, and μ_B is the Bohr magneton. γ is the spin relaxation rate, which results from various processes, such as spin-exchange collisions and atom-wall collisions [22]. The noise terms dW_i, with $i \in \{x, y, z\}$, arise from intrinsic spin fluctuations and are considered Gaussian white noise with zero mean and a variance of dt, i.e., $\langle dW_i(t)\rangle = 0$ and $\langle dW_i(\tau) dW_i(0)\rangle = \delta(\tau)dt$, with τ being the time lag [31]. The Gaussian distribution of $d\boldsymbol{W}$ arises from the central-limit theorem for a large number of independent atoms. The state-independent noise strength Q is $Q = \sqrt{2\gamma \mathrm{Var}(F_i)}$, with $\mathrm{Var}(F_i) = 4\hbar^2 N_{\rm at}$ being the variance of the collective angular momentum component, assuming the spin dynamics is a stationary noise process [38].

We probe the collective spins via their effect on the polarization of the laser beam, which we quantify via the Stokes vector $\boldsymbol{S} = (S_1, S_2, S_3)$; we have

$$\begin{aligned} S_1 &\equiv [n_{\rm ph}(x) - n_{\rm ph}(y)]/2, \\ S_2 &\equiv [n_{\rm ph}(+45^\circ) - n_{\rm ph}(-45^\circ)]/2, \\ S_3 &\equiv [n_{\rm ph}(\sigma_+) - n_{\rm ph}(\sigma_-)]/2. \end{aligned} \tag{2}$$

Here, $n_{\rm ph}$ represents the number of photons. The arguments x, y, and $\pm 45^\circ$ denote polarization along Cartesian axes, while $\sigma_\pm$ indicate left- and right-hand circular polarization. The indices 1,2,3 refer to the components of the Stokes vector. For the input laser beam, the component $S_1^{(\rm in)}$ can be approximated as a large classical value $S_1 = \langle S_1^{(\rm in)}(t)\rangle$, while the components $S_2^{(\rm in)}$ and $S_3^{(\rm in)}$ are considered to be Gaussian processes with zero mean, $\langle S_2^{(\rm in)}(t)\rangle = \langle S_3^{(\rm in)}(t)\rangle = 0$, and variance $\mathrm{Var}[S_2^{(\rm in)}(t)] = \mathrm{Var}[S_3^{(\rm in)}(t)] = S_1/2$ due to the commutation relation $[\hat{S}_2^{(\rm in)}, \hat{S}_3^{(\rm in)}] = i\hat{S}_1^{(\rm in)}$ [39].

On passing through the cell, the optical polarization experiences a rotation due to a difference in refractive index for left- and right-hand circular polarizations [40]. The effect can

be described by the Hamiltonian

$$\hat{H}_{\rm int} = G\hat{F}_z\hat{S}_3, \tag{3}$$

where F_z is the z component of the collective spin $\boldsymbol{F}$. The coupling coefficient is $G = -\frac{\hbar c a_1 \lambda^2 \Delta_l}{16\pi A_l \delta_l}$ [41]. Here, c is the speed of light, λ is the laser wavelength, A_l is the laser-beam cross section, and a_1 is the dimensionless vector polarizability. The interaction rotates the Stokes vector $\boldsymbol{S}$ around the three-axis by an amount proportional to $F_z(t)$. According to the Heisenberg equation of motion $d\hat{\boldsymbol{S}}/dt = i[\hat{H}_{\rm int}, \hat{\boldsymbol{S}}]/\hbar$, the polarization of the output laser beam can be expressed by the Stokes parameter formalism using the input-output relations

$$\begin{aligned} S_1^{(\rm out)}(t) &\approx S_1^{(\rm in)}(t), \\ S_2^{(\rm out)}(t) &\approx S_2^{(\rm in)}(t) + \frac{G}{\hbar c}F_z(t)S_1, \\ S_3^{(\rm out)}(t) &= S_3^{(\rm in)}(t). \end{aligned} \tag{4}$$

Therefore, the longitudinal component of the atomic angular momentum rotates the polarization of the laser beam.

If two laser beams travel through the same vapor cell without overlap, their polarization is modified by the atoms in their separate beam paths. In the following, we write $\boldsymbol{F}_a$ and $\boldsymbol{F}_b$ for the collective angular momenta of these ensembles. Since the atoms are free to travel through the cell, these two ensembles are correlated. When atoms uniformly redistribute throughout the entire cell much faster than the spin relaxation rate, the influence of the details of the atomic motion on spin dynamics and spin correlations can be neglected. The correlation can be quantified by the following set of stochastic Bloch equations [31,42]:

$$\begin{aligned} d\boldsymbol{F}_a =& (g_F\mu_B\boldsymbol{F}_a \times \boldsymbol{B} - \gamma\boldsymbol{F}_a - k_{ad}\boldsymbol{F}_a + k_{da}\boldsymbol{F}_d)dt \\ &+ \boldsymbol{Q}_{aa}d\boldsymbol{W}_a + \boldsymbol{Q}_{da}d\boldsymbol{W}_d, \\ d\boldsymbol{F}_b =& (g_F\mu_B\boldsymbol{F}_b \times \boldsymbol{B} - \gamma\boldsymbol{F}_b - k_{bd}\boldsymbol{F}_b + k_{db}\boldsymbol{F}_d)dt \\ &+ \boldsymbol{Q}_{bb}d\boldsymbol{W}_b + \boldsymbol{Q}_{db}d\boldsymbol{W}_d, \\ d\boldsymbol{F}_d =& [g_F\mu_B\boldsymbol{F}_d \times \boldsymbol{B} - \gamma\boldsymbol{F}_d - (k_{da}+k_{db})\boldsymbol{F}_d + k_{ad}\boldsymbol{F}_a \\ &+ k_{bd}\boldsymbol{F}_b]dt + \boldsymbol{Q}_{dd}d\boldsymbol{W}_d + \boldsymbol{Q}_{ad}d\boldsymbol{W}_a + \boldsymbol{Q}_{bd}d\boldsymbol{W}_b, \end{aligned} \tag{5}$$

where $\boldsymbol{F}_d$ denotes the collective angular momentum of the atoms outside of the laser beams. Here, $k_{\alpha\beta}$, with $\alpha, \beta \in \{a, b, d\}$, are the hopping rates from ensemble α to ensemble β and are shown as red arrows in Fig. 1(a). $\boldsymbol{Q}_{\alpha\beta}$, with $\alpha \in \{a, b, d\}$, depend on the angular momentum variance, the relaxation rate, and the hopping rate, as described by the fluctuation-dissipation theorem [see Eq. (A2) in the Appendix]. Here, we neglect the back-action of laser beams $\sim\langle F\rangle$ that is far less than the intrinsic spin noise $\sim\sqrt{\mathrm{Var}(F)}$ for the unpolarized atomic ensemble [31]. Under our experimental conditions, the cross-sectional area of both laser beams is $A_l \approx 10\,\mathrm{mm}^2$. We can therefore reduce the number of parameters by setting $k_{ad} = k_{bd} = k_a$ and $k_{da} = k_{db} = k_d$. The diameter of the laser beams is considerably smaller than that of the cell (35 mm); thus, $k_d/k_a \ll 1$. For the coated cell, the atoms can travel between the different ensembles without significant loss of the spin polarization, so $\gamma/k_a \ll 1$.

III. CORRELATION FUNCTIONS

To quantify the degree of synchronization between the two laser beams, we calculate the auto- and cross-correlation functions of the Stokes parameters [5]

$$g_{\alpha\beta}(\tau) = \left\langle S_{\alpha 2}^{(\rm out)}(\tau)S_{\beta 2}^{(\rm out)}(0)\right\rangle, \tag{6}$$

where $\alpha, \beta \in \{a, b\}$. According to Eq. (4), the polarizations depend on the input polarizations and the spin polarizations $F_{\alpha z}$ in the medium:

$$g_{\alpha\beta}(\tau) = \left\langle S_{\alpha 2}^{(\rm in)}(\tau)S_{\beta 2}^{(\rm in)}(0)\right\rangle + \frac{G^2S_1^2}{\hbar^2c^2}\langle F_{\alpha z}(\tau)F_{\beta z}(0)\rangle. \tag{7}$$

Here, we use the fact that $\langle S_2^{(\rm in)}(\tau)F_z(0)\rangle = 0$ because the input laser beams are not correlated to the spins. Considering $S_2^{(\rm in)}(t)$ to be a Gaussian noise process,

$$\left\langle S_{\alpha 2}^{(\rm in)}(\tau)S_{\beta 2}^{(\rm in)}(0)\right\rangle = \delta_{\alpha\beta}S_1\delta(\tau)/2. \tag{8}$$

Here, $\delta_{\alpha\beta}$ is the Kronecker delta function, and $\delta(\tau)$ is the Dirac delta function. The cross-correlation functions $\langle F_{\alpha z}(\tau)F_{\beta z}(0)\rangle$, with $\alpha, \beta \in \{a, b\}$, can be obtained from the dynamics in Eq. (5) as [see Eqs. (A3)–(A8) in the Appendix]

$$\langle F_{\alpha z}(\tau)F_{\beta z}(0)\rangle \approx \mathrm{Var}(F_z)\cos(\omega_L\tau)\left(\frac{k_d}{k_a}e^{-\gamma|\tau|} + \delta_{\alpha\beta}e^{-k_a|\tau|}\right). \tag{9}$$

Combining the correlation functions in Eqs. (8) and (9) with Eq. (7), we obtain the correlation spectra $\tilde{g}_{\alpha\beta}(\omega)$ from the Fourier transform of $g_{\alpha\beta}(\tau)$:

$$\begin{aligned} \tilde{g}_{\alpha\beta}(\omega) =& \frac{4G^2S_1^2N_{\rm at}}{c^2}\left[\frac{k_d}{k_a}\frac{\gamma}{(\omega-\omega_L)^2+\gamma^2} + \frac{\delta_{\alpha\beta}k_a}{(\omega-\omega_L)^2+k_a^2}\right] \\ &+ \frac{\delta_{\alpha\beta}S_1}{2}. \end{aligned} \tag{10}$$

From Eq. (10), we can see that the autocorrelation spectrum $\tilde{g}_{aa}(\omega) = \tilde{g}_{bb}(\omega)$ consists of three components: a narrow peak at ω_L with a half width at half maximum (HWHM) equal to γ (the first term), a broad peak at ω_L with a HWHM equal to k_a (the second term), and a photon shot-noise base with a height of $S_1/2$ (the third term, a fundamental limit to the optical detection). The cross-correlation spectrum $\tilde{g}_{ab}(\omega) = \tilde{g}_{ba}(\omega)$ exhibits a peak only at ω_L with a HWHM equal to γ. Therefore, the cross-correlation spectrum is equal to the first term of the autocorrelation spectrum. The result indicates that after times $\gg 1/k_a$, the atoms have traveled distances that are large compared to the beam diameter and the distance between the beams. The cross-correlation spectrum characterizes the synchronization of the two output laser beams mediated by the atomic spins simultaneously flying through both beams during the decoherence time.

The cross-correlation spectrum $\tilde{g}_{ab}(\omega)$ or $\tilde{g}_{ba}(\omega)$ is a complex number whose normalized amplitude is [5]

$$C_{ab}(\omega) = \frac{|\tilde{g}_{ab}(\omega)|}{\sqrt{\tilde{g}_{aa}(\omega)}\sqrt{\tilde{g}_{bb}(\omega)}}, \tag{11}$$

and its phase is

$$\Psi_{ab}(\omega) = \arctan\left\{\frac{\mathrm{Im}[\tilde{g}_{ab}(\omega)]}{\mathrm{Re}[\tilde{g}_{ab}(\omega)]}\right\}. \tag{12}$$

The amplitude measures the synchronization between two signals, i.e., $S_{a2}^{(\mathrm{out})}(t)$ and $S_{b2}^{(\mathrm{out})}(t)$, as a function of the frequency ω, which ranges from 0 (no correlation) to 1 (perfect correlation). When $\omega = \omega_L$, $\Psi_{ab} \approx 0$, indicating nearly in phase synchronization. With Eq. (10), the correlation amplitude at the Larmor frequency becomes

$$C_{ab}(\omega_L) = \frac{8G^2 S_1 N_{\mathrm{at}} k_d}{8G^2 S_1 N_{\mathrm{at}}(\gamma + k_d) + c^2 k_a \gamma}. \tag{13}$$

The number of atoms inside the beam N_{at} varies with the vapor temperature T_v as [43]

$$N_{\mathrm{at}} \approx 0.722 \frac{7}{12} \frac{A_l l}{T_v} 10^{14.178 - 4040/T_v}, \tag{14}$$

where the coefficient 0.722 denotes the natural abundance of ^{85}Rb, the coefficient $7/12$ represents the fraction of atoms on the $F = 3$ level, and l is the cell length. This can be used to adjust the degree of correlation.

IV. EXPERIMENTAL DEMONSTRATION

We perform the experiment on the setup shown in Fig. 1(a). Two laser beams, sourced from independent laser diodes with 1-mW power, are transversely separated by approximately 5 mm, each with an effective beam diameter of about 3 mm. They are sent through an OTS-coated cell filled with unpolarized ^{85}Rb atoms. The vapor cell is shielded by a five-layer μ-metal shield, reducing the residual magnetic field to less than 1 nT. Inside the shield, a solenoid coil generates the uniform magnetic field $\boldsymbol{B} = (0, B, 0)$. The vapor temperature is maintained by an oven, ranging from 285.7 to 359.3 K. After two laser beams pass through the vapor cell, we simultaneously measure their respective Stokes components $S_{a2}^{(\mathrm{out})}(t)$ and $S_{b2}^{(\mathrm{out})}(t)$ by independent balanced photodiodes, and then the signals are simultaneously digitized by a multichannel data acquisition card (NI 9223). Finally, the correlation spectra of the Stokes component $S_2^{(\mathrm{out})}(t)$ of two laser beams are calculated from the recorded time-domain data.

Figure 2(c) shows the auto- and cross-correlation spectra $|\tilde{g}_{aa}(\omega)|$ and $|\tilde{g}_{ab}(\omega)|$ at a vapor temperature of 342.0 K. Here, we use their amplitudes, which are very close to the real part. In the ideal case, the imaginary part vanishes, but in the experimental data, we find small signals below the experimental uncertainty. We overlay the theoretical and experimental spectra to make a comparison. The autocorrelation spectrum exhibits a narrow spin-noise peak at the Larmor frequency $\omega_L = 163.3$ kHz with a HWHM equal to $\gamma = 42\ \mathrm{s}^{-1}$, a broad spin-noise peak at ω_L with a HWHM equal to $k_a = 4.4 \times 10^4\ \mathrm{s}^{-1}$, and a photon shot-noise base. The cross-correlation spectrum manifests a narrow peak at ω_L. The line shapes of the experimental auto- and cross-correlation spectra are in good agreement with those of the theoretical spectra calculated from Eq. (10), thereby validating our model. The small peak at 163.5 kHz matches the Larmor frequency expected for the $F = 2$ subsystem if the nuclear Zeeman effect is taken into account. We conclude that the synchronization scheme does not depend on the hyperfine state. The signal from $F = 3$ is nearly an order of magnitude larger than that of $F = 2$, as expected from the different detunings (see Sec. II).

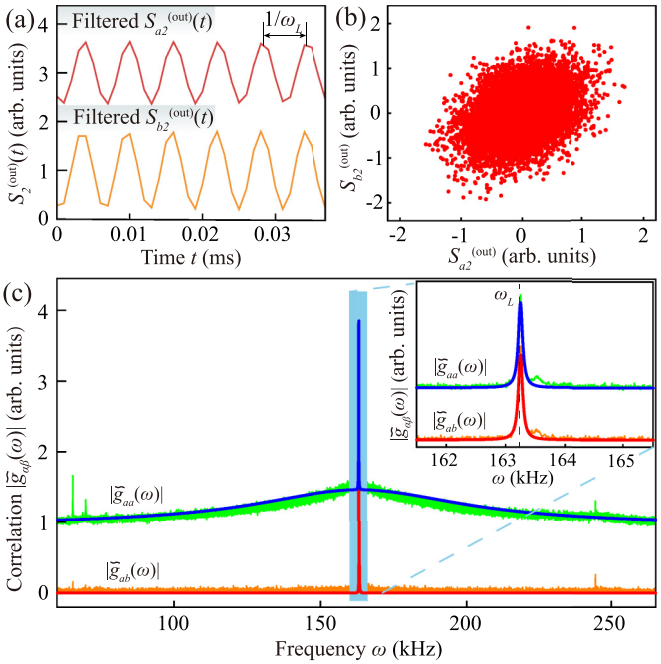

FIG. 2. Experimental Stokes components $S_2^{(\mathrm{out})}(t)$ of the two output laser beams and their correlation. (a) Measured Stokes components $S_2^{(\mathrm{out})}(t)$ of the two laser beams after applying a band-pass filter centered at the Larmor frequency ω_L, with a bandwidth of 500 Hz. During the interval shown here, the two signals are synchronized in phase. (b) Correlation plot between the filtered Stokes components $S_2^{(\mathrm{out})}(t)$. The data points shown here correspond to a time slice of 100 s; the correlation coefficient is about 0.34. (c) Theoretical and experimental auto- and cross-correlation spectra. The cross-correlation peak indicates the synchronization at ω_L between the two laser beams. Line shapes of both experimental auto- and cross- correlation spectra (noisy curves) are in good agreement with the theoretical expectations (smooth curves) derived from Eq. (10), validating the theoretical model. The inset shows the zoomed-in correlation spectra around ω_L.

We can quantify the synchronization by the cross-correlation amplitude $C_{ab}(\omega)$ and the phase $\Psi_{ab}(\omega)$, which are shown in Figs. 3(a) and 3(b), respectively. We obtain $C_{ab}(\omega_L) = 0.65$, and $\Psi_{ab}(\omega_L) = 0.06$ rad, which confirms the nearly in phase synchronization at ω_L between the two laser beams. At other frequencies, $C_{ab}(\omega)$ is indistinguishable from zero, and $\Psi_{ab}(\omega)$ fluctuates randomly. Moreover, we can determine k_d as $k_d = 198\ \mathrm{s}^{-1}$. The values of γ, k_d, and k_a validate assumptions in deriving Eq. (9), specifically $k_d/k_a \ll 1$ and $\gamma/k_a \ll 1$.

A comparative experiment is conducted in a cell filled with about 13 kPa of nitrogen buffer gas, where the atomic motion becomes diffusive and too slow for traveling between the two bright regions before the spins decohere. Figures 3(c) and 3(d) depict $C_{ab}(\omega)$ and $\Psi_{ab}(\omega)$, respectively, for this case. $C_{ab}(\omega)$ exhibits zero values, and $\Psi_{ab}(\omega)$ shows random behaviors, indicating the lack of synchronizations between two laser beams. The experimental results can be obtained by setting $k_d \to 0$ in the theoretical calculations. The results confirm the importance of spin hoppings in the synchronization scheme.

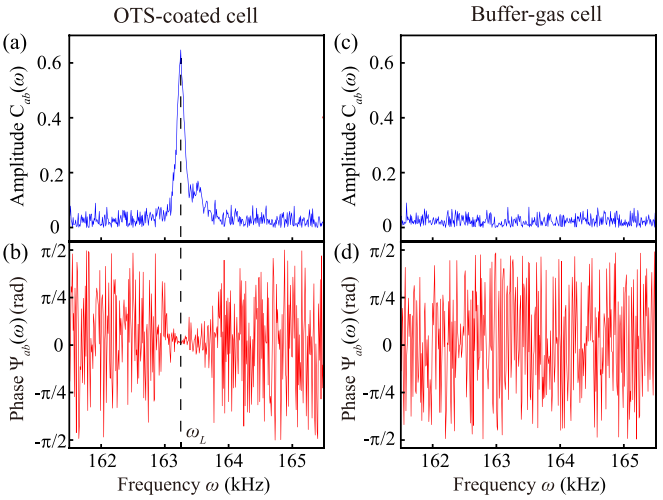

FIG. 3. Representative cross-correlation amplitudes $C_{ab}(\omega)$ and phases $\Psi_{ab}(\omega)$ for two independent laser beams. (a) and (b) show $C_{ab}(\omega)$ and $\Psi_{ab}(\omega)$, respectively, for the scenario where two laser beams become synchronized at ω_L. (c) and (d) illustrate $C_{ab}(\omega)$ and $\Psi_{ab}(\omega)$, respectively, for the case where buffer gas prevents the atoms from becoming correlated throughout the cell. As a result, the two laser beams remain independent.

According to the theory, we expect that the synchronization should occur at the Larmor frequency $\omega_L = g_F \mu_B B$, and the values $C_{ab}(\omega_L)$ and $\Psi_{ab}(\omega_L) = 0$ should be independent of B. We test this prediction by repeating the measurement at different magnetic fields. The results are shown in Fig. 4(a), where the magnetic-field strength is varied to cover Larmor frequencies from 106 to 277 kHz. Black triangles are experimental values of $C_{ab}(\omega_L)$, and the green shading represents the standard deviation, which is 3.4% in our experimental data. Red diamonds denote experimental values of $\Psi_{ab}(\omega_L)$, with a mean value of 0.12. The cyan shading indicates a standard deviation of 0.06. These deviations mainly arise from the technique noise and the atom-light interaction fluctuations induced by optical detuning fluctuations of about 0.05 GHz. The results demonstrate the stability of the synchronization over the wide synchronization frequency range.

According to Eq. (13), the correlation should increase with the number of atoms. We verify this prediction by adjusting

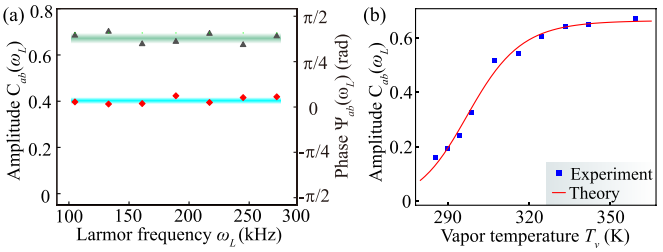

FIG. 4. (a) Synchronization for different Larmor frequencies ω_L. Black triangles represent the correlation amplitude $C_{ab}(\omega_L)$, and red diamonds represent the phases $\Psi_{ab}(\omega_L)$. The green shading and cyan shading are their standard deviations. (b) $C_{ab}(\omega_L)$ versus vapor temperature T_v. Blue squares represent the experimental results, while the red line is the theoretical expectation.

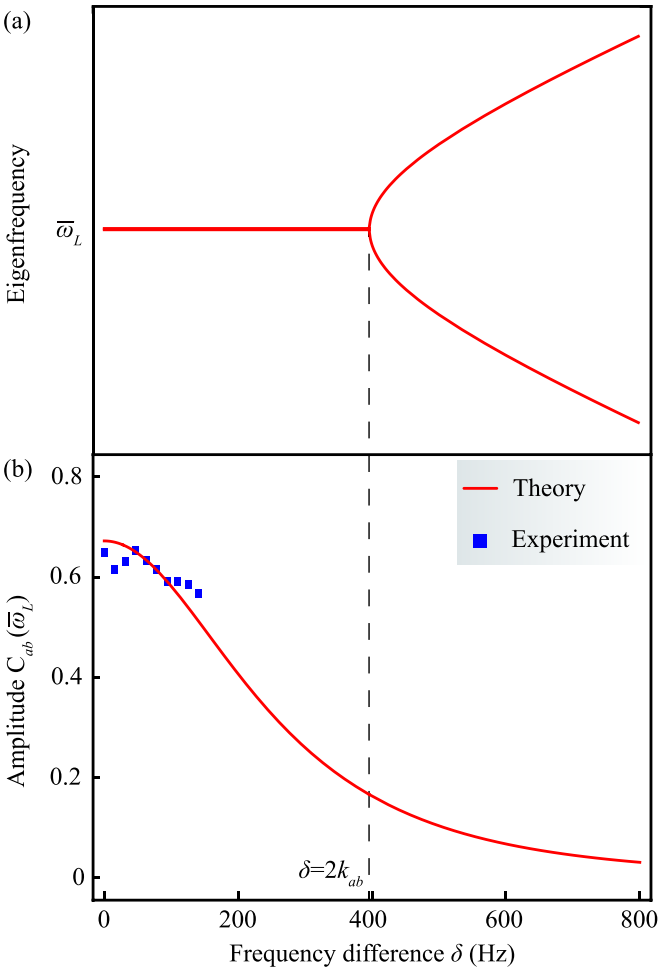

FIG. 5. (a) The eigenfrequency of the system versus the difference between the Larmor frequencies $\delta = \omega_{aL} - \omega_{bL}$. (b) The amplitude $C_{ab}(\bar{\omega}_L)$ as a function of δ. The hopping rate k_{ab} is approximated as $k_{ab} \approx k_d$ due to the relation for the hopping time $1/k_{ab} = 1/k_a + 1/k_d$, where $k_d = 198\ \mathrm{s}^{-1}$ is estimated from the experimental data shown in Fig. 2(c).

the temperature of the vapor cell and therefore the number of atoms $N_{\mathrm{at}}(T_v)$ in the laser beams. Figure 4(b) shows $C_{ab}(\omega_L)$ for the temperature range from 285.7 to 359.3 K at a constant Larmor frequency $\omega_L = 163.3$ kHz. The blue squares and the red line depict experimental and theoretical results, respectively. $C_{ab}(\omega_L)$ shows a rapid increase between 285.7 and 333.3 K and saturates at $k_d/(k_d + \gamma) \approx 0.66$ beyond 333.3 K, as determined by the best fit. Experimental results meet predictions well, suggesting that better synchronization requires a higher vapor temperature within a certain temperature range.

So far, we have assumed that the atoms in the two laser beams precess at the same Larmor frequency. As an interesting extension, we now consider the case where $\boldsymbol{F}_a$ and $\boldsymbol{F}_b$ have distinct Larmor frequencies, $\omega_{aL} = g_F \mu_B B_a$ and $\omega_{bL} = g_F \mu_B B_b$, respectively, but the atoms still exchange between the two regions. Figure 5(a) depicts the eigenfrequency of the system as a function of the frequency difference $\delta = \omega_{aL} - \omega_{bL}$, and Fig. 5(b) shows the amplitude $C_{ab}(\bar{\omega}_L)$ as a function of δ with the average Larmor frequency $\bar{\omega}_L = (\omega_{aL} + \omega_{bL})/2$. Here, we apply a small magnetic field

gradient in the y direction to make the Larmor frequencies of two ensembles different. When $\delta < 2k_{ab}$, the eigenfrequency of the system is a single frequency $\bar{\omega}_L$ [see Eqs. (A14) and (A15) in the Appendix]. The amplitude $C_{ab}(\bar{\omega}_L)$ remains significantly nonzero. Here, k_{ab} is the hopping rate between ensembles a and b. Therefore, the corresponding hopping time is approximately $1/k_{ab}$, which can also be expressed as approximately $1/k_a + 1/k_d$ when considering it as in the previous section. Thus, k_{ab} is approximated as $k_{ab} \approx k_d = 198\ \mathrm{s}^{-1}$. γ depends quadratically on δ [see Eq. (A27) in the Appendix]. For $\delta > 2k_{ab}$, the system bifurcates, and the eigenfrequencies are $\bar{\omega}_L \pm \sqrt{\delta^2/4 - k_{ab}^2}$ [see Eq. (A16) in the Appendix]. $C_{ab}(\bar{\omega}_L)$ becomes small. The experimental results, shown as the blue squares in Fig. 5(b), are in good agreement with the predicted trend. The results indicate that the synchronization scheme remains effective even when two laser beams respectively interact with collective spins having different Larmor frequencies.

V. CONCLUSION AND DISCUSSION

In conclusion, we proposed and demonstrated a different approach for achieving synchronization between spatially separated laser beams by atomic spin noise. The synchronization occurs in a narrow frequency band centered at the Larmor frequency of the atoms. The synchronization frequency can therefore be controlled and varied across a wide frequency range. The amplitude of the correlation function increases with the atomic density, which can be controlled by the vapor temperature. We also considered the case where the Larmor frequencies in the regions of the two laser beams are different. In this case, the correlation remains effective.

Our scheme creates two synchronized random laser beams. The input laser beams are detuned from atomic transitions, and therefore, the output beams still maintain notable intensity. This correlated randomness can be transmitted to distant locations by the laser beams, which opens the potential for applications such as long-range key distribution [11,44]. The unpredictability of random beams generated by our strategy relies on the inherent randomness of quantum spin noise, which is unpredictable in principle [18]. In the situation where the Larmor frequencies of the two interaction regions are different, our results suggest a critical point at $\delta = 2k_{ab}$, which usually indicates the occurrence of a phase transition [42,45]. Our experiment provides a potential platform for studying phase-transition phenomena, such as transitions between unbroken and broken phases in non-Hermitian physics [42,45].

ACKNOWLEDGMENTS

We thank K. Zhao for providing us with the OTS-coated cell. We thank H. Shen for valuable discussions. This work was supported by the Innovation Program for Quantum Science and Technology (Grant No. 2021ZD0303205), the National Natural Science Foundation of China (Grants No. 12261160569, No. 12150014, and No. 11927811), the Anhui Initiative in Quantum Information Technologies (Grant No. AHY050000), and the National Natural Science Foundation of China/Hong Kong RGC Collaborative Research Scheme (Project No. CRS CUHK401/22).

APPENDIX

1. Correlation between atomic ensembles with same Larmor frequency

Based on Eq. (5), the angular momentum vector $\boldsymbol{F} \equiv [F_{ax}, F_{ay}, F_{az}, F_{bx}, F_{by}, F_{bz}, F_{dx}, F_{dy}, F_{dz}]^T$ satisfies the stochastic differential equation

$$d\boldsymbol{F} = \boldsymbol{A}\boldsymbol{F}dt + \boldsymbol{Q}d\boldsymbol{W}, \tag{A1}$$

with

$$\boldsymbol{A} = \begin{bmatrix}
-\gamma - k_{ad} & 0 & -\omega_L & 0 & 0 & 0 & k_{da} & 0 & 0 \\
0 & -\gamma - k_{ad} & 0 & 0 & 0 & 0 & 0 & k_{da} & 0 \\
\omega_L & 0 & -\gamma - k_{ad} & 0 & 0 & 0 & 0 & 0 & k_{da} \\
0 & 0 & 0 & -\gamma - k_{bd} & 0 & -\omega_L & k_{db} & 0 & 0 \\
0 & 0 & 0 & 0 & -\gamma - k_{bd} & 0 & 0 & k_{db} & 0 \\
0 & 0 & 0 & \omega_L & 0 & -\gamma - k_{bd} & 0 & 0 & k_{db} \\
k_{ad} & 0 & 0 & k_{bd} & 0 & 0 & -\gamma - k_{da} - k_{db} & 0 & -\omega_L \\
0 & k_{ad} & 0 & 0 & k_{bd} & 0 & 0 & -\gamma - k_{da} - k_{db} & 0 \\
0 & 0 & k_{ad} & 0 & 0 & k_{bd} & \omega_L & 0 & -\gamma - k_{da} - k_{db}
\end{bmatrix}$$

and the noise vector $d\boldsymbol{W} \equiv [dW_{ax}, dW_{ay}, dW_{az}, dW_{bx}, dW_{by}, dW_{bz}, dW_{dx}, dW_{dy}, dW_{dz}]^T$. If the spin dynamics is a stationary noise process [38], then the noise strength matrix $\boldsymbol{Q}$ satisfies [31,46]

$$\boldsymbol{A}\boldsymbol{\sigma}(0) + \boldsymbol{\sigma}(0)\boldsymbol{A}^T = -\boldsymbol{Q}\boldsymbol{Q}^T, \tag{A2}$$

where $\boldsymbol{\sigma}(\tau) = \langle \boldsymbol{F}(t+\tau)\boldsymbol{F}^T(t)\rangle_t$ is the time-correlation matrix with $\langle\cdot\rangle_t$ the average over t.

The evolution of $\boldsymbol{\sigma}(\tau)$ ($\tau \neq 0$) satisfies [31]

$$\begin{aligned}
\frac{d}{d\tau}\boldsymbol{\sigma}(\tau) &= \left\langle \frac{\boldsymbol{A}\boldsymbol{F}(t+\tau)d\tau + \boldsymbol{Q}d\boldsymbol{W}(t+\tau)}{d\tau}\boldsymbol{F}^T(t)\right\rangle_t \\
&= \boldsymbol{A}\langle \boldsymbol{F}(t+\tau)\boldsymbol{F}(t)^T\rangle_t + \boldsymbol{Q}\frac{\langle d\boldsymbol{W}(t+\tau)\boldsymbol{F}^T(t)\rangle_t}{d\tau} \\
&= \boldsymbol{A}\boldsymbol{\sigma}(\tau),
\end{aligned} \tag{A3}$$

where we assume there is no correlation between the noise term $d\boldsymbol{W}(t+\tau)(\tau \neq 0)$ and the angular momentum $\boldsymbol{F}^T(t)$. Consequently, the time correlation matrix for $\tau > 0$ is

$$\boldsymbol{\sigma}(\tau) = \exp(\boldsymbol{A}\tau)\boldsymbol{\sigma}(0). \tag{A4}$$

Since $\boldsymbol{A}$ is not a diagonal matrix, it is convenient to diagonalize $\boldsymbol{A}$ to obtain the matrix exponential $\exp(\boldsymbol{A}\tau)$. The matrix $\boldsymbol{A}$ can be diagonalized into

$$\boldsymbol{A} = \boldsymbol{V}\boldsymbol{\Lambda}\boldsymbol{V}^{-1}, \tag{A5}$$

with the matrix $\boldsymbol{\Lambda} = \mathrm{diag}[-\gamma, -\gamma - k_a, -\gamma - k_a - 2k_d, -\gamma - i\omega_L, -\gamma - k_a - i\omega_L, -\gamma - k_a - 2k_d - i\omega_L, -\gamma + i\omega_L, -\gamma - k_a + i\omega_L, -\gamma - k_a - 2k_d + i\omega_L]$ and the eigenvectors

$$\boldsymbol{V} = \begin{bmatrix}
0 & 0 & 0 & -i\frac{k_d}{k_a} & i & \frac{i}{2} & \frac{k_d}{k_a} & -i & -\frac{i}{2} \\
\frac{k_d}{k_a} & -1 & -\frac{1}{2} & 0 & 0 & 0 & 0 & 0 & 0 \\
0 & 0 & 0 & \frac{k_d}{k_a} & -1 & -\frac{1}{2} & \frac{k_d}{k_a} & -1 & -\frac{1}{2} \\
0 & 0 & 0 & -i\frac{k_d}{k_a} & -i & \frac{i}{2} & i\frac{k_d}{k_a} & i & -\frac{i}{2} \\
\frac{k_d}{k_a} & 1 & -\frac{1}{2} & 0 & 0 & 0 & 0 & 0 & 0 \\
0 & 0 & 0 & \frac{k_d}{k_a} & 1 & -\frac{1}{2} & \frac{k_d}{k_a} & 1 & -\frac{1}{2} \\
0 & 0 & 0 & -i & 0 & -i & i & 0 & i \\
1 & 0 & 1 & 0 & 0 & 0 & 0 & 0 & 0 \\
0 & 0 & 0 & 1 & 0 & 1 & 1 & 0 & 1
\end{bmatrix},$$

Here, we use $k_{ad} = k_{bd} = k_a$ and $k_{da} = k_{db} = k_d$ to reduce the number of parameters, assuming the cross-sectional areas of two beams are equal. Since the number of atoms in a region should be conserved, $k_a/k_d = N_{\mathrm{at}}^{(d)}/N_{\mathrm{at}}^{(a)}$, with $N_{\mathrm{at}}^{(\alpha)}$ being the number of atoms in region α, where $\alpha \in \{a, d\}$. Then the matrix exponential $\exp(\boldsymbol{A}\tau)$ is

$$\exp(\boldsymbol{A}\tau) = \boldsymbol{V}\exp(\boldsymbol{\Lambda}\tau)\boldsymbol{V}^{-1}. \tag{A6}$$

The initial state of the time correlation matrix is calculated by $\boldsymbol{\sigma}(0) = \sum_m \rho_m \langle m|\hat{F}\hat{F}^\dagger|m\rangle = \mathrm{diag}[\mathrm{Var}(F_{ax}), \mathrm{Var}(F_{ay}), \mathrm{Var}(F_{az}), \mathrm{Var}(F_{bx}), \mathrm{Var}(F_{by}), \mathrm{Var}(F_{bz}), \mathrm{Var}(F_{dx}), \mathrm{Var}(F_{dy}), \mathrm{Var}(F_{dz})]$, where $|m\rangle$ is the eigenvector of the spin Hamiltonian and ρ_m is the occupation factor of $|m\rangle$ at the thermal equilibrium. Thus, according to Eq. (A4), the correlation functions $\langle F_{\alpha z}(\tau)F_{\beta z}(0)\rangle$, with $\alpha, \beta \in \{a, b\}$, are

$$\langle F_{\alpha z}(\tau)F_{\beta z}(0)\rangle = \begin{cases} \left[\frac{1}{2}e^{-(\gamma+k_a+2k_d)\tau} - \frac{k_a+2k_d}{2k_a}e^{-(\gamma+k_a+2k_d)\tau} + \frac{k_d}{k_a}e^{-\gamma\tau}\right]\mathrm{Var}(F_z)\cos(\omega\tau), & \alpha \neq \beta, \\ \left[\frac{1}{2}e^{-(\gamma+k_a+2k_d)\tau} + \frac{k_a+2k_d}{2k_a}e^{-(\gamma+k_a+2k_d)\tau} + \frac{k_d}{k_a}e^{-\gamma\tau}\right]\mathrm{Var}(F_z)\cos(\omega\tau), & \alpha = \beta. \end{cases} \tag{A7}$$

Here, we simplify $\mathrm{Var}(F_{az})$ and $\mathrm{Var}(F_{bz})$ as $\mathrm{Var}(F_z)$. Since the cross-sectional area of the laser beams is considerably smaller than that of the cell, we have $k_d/k_a \ll 1$. The atoms can travel between the different ensembles without significant loss of the spin polarization in the coated cell, so $\gamma/k_a \ll 1$. Therefore, we can approximate $\langle F_{\alpha z}(\tau)F_{\beta z}(0)\rangle$ as

$$\langle F_{\alpha z}(\tau)F_{\beta z}(0)\rangle \approx \mathrm{Var}(F_z)\cos(\omega_L\tau)\left(\frac{k_d}{k_a}e^{-\gamma\tau} + \delta_{\alpha\beta}e^{-k_a\tau}\right). \tag{A8}$$

Moreover, we find that the components F_{ay} and F_{by}, which are along the direction of the magnetic field, have no impact on $\langle F_{\alpha z}(\tau)F_{\beta z}(0)\rangle$ based on Eq. (A4). Therefore, we ignore these two components in the following calculations.

2. Correlation between atomic ensembles with different Larmor frequencies

If we replace the Larmor frequency ω_L with $\omega_{\alpha L} = g_F\mu_B B_\alpha$ for the Larmor frequencies of $\boldsymbol{F}_\alpha$, where $\alpha \in \{a, b, d\}$, in Eq. (5), obtaining its analytical solution necessitates solving a univariate sextic equation, thus rendering a general analytical solution unattainable. To derive an analytical conclusion, we omit the atoms in the dark region d and simplify the dynamics of collective angular momenta as

$$\begin{aligned} d\boldsymbol{F}_a &= (g_F\mu_B\boldsymbol{F}_a \times \boldsymbol{B}_a - \gamma\boldsymbol{F}_a - k_{ab}\boldsymbol{F}_a + k_{ba}\boldsymbol{F}_b)dt \\ &\quad + \boldsymbol{Q}'_{aa}d\boldsymbol{W}'_a + \boldsymbol{Q}'_{ba}d\boldsymbol{W}'_b, \\ d\boldsymbol{F}_b &= (g_F\mu_B\boldsymbol{F}_b \times \boldsymbol{B}_b - \gamma\boldsymbol{F}_b - k_{ba}\boldsymbol{F}_b + k_{ab}\boldsymbol{F}_a)dt \\ &\quad + \boldsymbol{Q}'_{bb}d\boldsymbol{W}'_b + \boldsymbol{Q}'_{ab}d\boldsymbol{W}'_a. \end{aligned} \tag{A9}$$

Here, k_{ab} and k_{ba} are effective hopping rates between $\boldsymbol{F}_a$ and $\boldsymbol{F}_b$. To distinguish from the case where the atoms have the same Larmor frequency, we use the primed symbols to describe the spin dynamics in this scenario as

$$d\boldsymbol{F}' = \boldsymbol{A}'\boldsymbol{F}'dt + \boldsymbol{Q}'d\boldsymbol{W}', \tag{A10}$$

with the angular momentum vector $\boldsymbol{F}' \equiv [F_{ax}, F_{az}, F_{bx}, F_{bz}]^T$, the rate matrix

$$\boldsymbol{A}' = \begin{bmatrix} -\gamma - k_{ab} & -\omega_{aL} & k_{ba} & 0 \\ \omega_{aL} & -\gamma - k_{ab} & 0 & k_{ba} \\ k_{ab} & 0 & -\gamma - k_{ba} & -\omega_{bL} \\ 0 & k_{ab} & \omega_{bL} & -\gamma - k_{ba} \end{bmatrix},$$

and the noise vector $d\boldsymbol{W'} \equiv [dW'_{ax}, dW'_{az}, dW'_{bx}, dW'_{bz}]^T$. The noise strength matrix $\boldsymbol{Q'}$ satisfies

$$\boldsymbol{A'\sigma'}(0) + \boldsymbol{\sigma'}(0)\boldsymbol{A'}^T = -\boldsymbol{Q'Q'}^T, \tag{A11}$$

where $\boldsymbol{\sigma'}(\tau) = \langle \boldsymbol{F'}(t+\tau)\boldsymbol{F'}^T(t)\rangle_t$. According to Eq. (7), we need to calculate $\langle F_{\alpha z}(\tau)F_{\beta z}(0)\rangle$ to obtain the correlation function $g_{\alpha\beta}(\tau)$. The initial state of the time correlation matrix is $\boldsymbol{\sigma'}(0) = \mathrm{diag}[\mathrm{Var}(F_{ax}), \mathrm{Var}(F_{az}), \mathrm{Var}(F_{bx}), \mathrm{Var}(F_{bz})]$. Similar to Eq. (A4), the time correlation matrix $\boldsymbol{\sigma'}(\tau)$ $(\tau > 0)$ is calculated as

$$\boldsymbol{\sigma'}(\tau) = \exp(\boldsymbol{A'}\tau)\boldsymbol{\sigma'}(0), \tag{A12}$$

where the matrix $\boldsymbol{A'}$ can be diagonalized into

$$\boldsymbol{A'} = \boldsymbol{V'\Lambda'V'}^{-1}. \tag{A13}$$

Here, $\boldsymbol{\Lambda'} = \mathrm{diag}[-\gamma - k_{ab} - \Delta + i\bar{\omega}_L, -\gamma - k_{ab} + \Delta - i\bar{\omega}_L, -\gamma - k_{ab} - \Delta - i\bar{\omega}_L, -\gamma - k_{ab} + \Delta + i\bar{\omega}_L]$. The average Larmor frequency is $\bar{\omega}_L = (\omega_{aL} + \omega_{bL})/2$, and the difference $\delta = \omega_{aL} - \omega_{bL}$. The behavior of the system depends on the relative size of this frequency difference and the exchange rates k_{ab}. It can be quantified by the parameter $\Delta = \sqrt{k_{ab}^2 - \delta^2/4}$. From the detailed balance, $k_{ab} = k_{ba}$. Δ^2 determines the values of the matrices $\boldsymbol{\Lambda'}$ and $\boldsymbol{V'}$ and therefore determines the correlation matrix $\boldsymbol{\sigma'}(\tau)$.

Next, we categorically analyze $\boldsymbol{\sigma'}(\tau)$ with respect to whether Δ is a real or imaginary number. For the case where Δ is real and the hopping between the two ensembles is faster than the differential precession, the correlation functions $\langle F_{\alpha z}(\tau)F_{\beta z}(0)\rangle$ $(\tau > 0)$, with $\alpha, \beta \in \{a, b\}$, are

$$\begin{aligned}
\langle F_{az}(\tau)F_{az}(0)\rangle &= \mathrm{Var}(F_z)\frac{e^{-(\gamma+k_{ab})\tau}}{2\Delta}[|\delta|(e^{-\Delta\tau} - e^{\Delta\tau})\sin(\bar{\omega}_L t) + \Delta(e^{-\Delta\tau} + e^{\Delta\tau})\cos(\bar{\omega}_L\tau)],\\
\langle F_{bz}(\tau)F_{bz}(0)\rangle &= \mathrm{Var}(F_z)\frac{e^{-(\gamma+k_{ab})\tau}}{2\Delta}[|\delta|(e^{\Delta\tau} - e^{-\Delta\tau})\sin(\bar{\omega}_L t) + \Delta(e^{-\Delta\tau} + e^{\Delta\tau})\cos(\bar{\omega}_L\tau)],\\
\langle F_{az}(\tau)F_{bz}(0)\rangle &= \mathrm{Var}(F_z)\frac{e^{-(\gamma+k_{ab})\tau}}{2\Delta}k_{ab}(e^{\Delta\tau} - e^{-\Delta\tau})\cos(\bar{\omega}_L\tau).
\end{aligned} \tag{A14}$$

Combining Eqs. (7), (8), and (A14), we obtain the correlation spectra of the two laser beams as

$$\begin{aligned}
\tilde{g}_{aa}(\omega) =& \frac{2G^2S_1^2N_{\mathrm{at}}}{c^2}\left[\frac{|\delta|}{\Delta}\frac{\bar{\omega}_L - \omega}{(\omega-\bar{\omega}_L)^2 + (\gamma + k_{ab} + \Delta)^2} - \frac{|\delta|}{\Delta}\frac{\bar{\omega}_L - \omega}{(\omega-\bar{\omega}_L)^2 + (\gamma + k_{ab} - \Delta)^2}\right.\\
&\left. + \frac{\gamma + k_{ab} + \Delta}{(\omega-\bar{\omega}_L)^2 + (\gamma + k_{ab} + \Delta)^2} + \frac{\gamma + k_{ab} - \Delta}{(\omega-\bar{\omega}_L)^2 + (\gamma + k_{ab} - \Delta)^2}\right] + \frac{S_1}{2},\\
\tilde{g}_{bb}(\omega) =& \frac{2G^2S_1^2N_{\mathrm{at}}}{c^2}\left[\frac{|\delta|}{\Delta}\frac{\bar{\omega}_L - \omega}{(\omega-\bar{\omega}_L)^2 + (\gamma + k_{ab} - \Delta)^2} - \frac{|\delta|}{\Delta}\frac{\bar{\omega}_L - \omega}{(\omega-\bar{\omega}_L)^2 + (\gamma + k_{ab} + \Delta)^2}\right.\\
&\left. + \frac{\gamma + k_{ab} + \Delta}{(\omega-\bar{\omega}_L)^2 + (\gamma + k_{ab} + \Delta)^2} + \frac{\gamma + k_{ab} - \Delta}{(\omega-\bar{\omega}_L)^2 + (\gamma + k_{ab} - \Delta)^2}\right] + \frac{S_1}{2},\\
\tilde{g}_{ab}(\omega) =& \frac{2G^2S_1^2N_{\mathrm{at}}}{c^2}\frac{k_{ab}}{\Delta}\left[\frac{\gamma + k_{ab} - \Delta}{(\omega-\bar{\omega}_L)^2 + (\gamma + k_{ab} - \Delta)^2} - \frac{\gamma + k_{ab} + \Delta}{(\omega-\bar{\omega}_L)^2 + (\gamma + k_{ab} + \Delta)^2}\right].
\end{aligned} \tag{A15}$$

Thus, the polarizations of the laser beams oscillate and synchronize at $\bar{\omega}_L$.

For the case where Δ is imaginary and the hopping between the two ensembles is slower than the differential precession, the system bifurcates, and the eigenvalues become $\boldsymbol{\Lambda'} = \mathrm{diag}[-\gamma - k_{ab} + i(\bar{\omega}_L - \epsilon), -\gamma - k_{ab} - i(\bar{\omega}_L - \epsilon), -\gamma - k_{ab} - i(\bar{\omega}_L + \epsilon), -\gamma - k_{ab} + i(\bar{\omega}_L + \epsilon)]$, with $\epsilon = -i\Delta$. Based on Eqs. (A12) and (A13), the correlation functions $\langle F_{\alpha z}(\tau)F_{\beta z}(0)\rangle$ $(\tau > 0)$, with $\alpha, \beta \in \{a, b\}$, are

$$\begin{aligned}
\langle F_{az}(\tau)F_{az}(0)\rangle =& \mathrm{Var}(F_z)\left\{\frac{2\epsilon + |\delta|}{4\epsilon}\cos[(\bar{\omega}_L + \epsilon)\tau] + \frac{2\epsilon - |\delta|}{4\epsilon}\cos[(\bar{\omega}_L - \epsilon)\tau]\right\}e^{-(\gamma+k_{ab})\tau},\\
\langle F_{bz}(\tau)F_{bz}(0)\rangle =& \mathrm{Var}(F_z)\left\{\frac{2\epsilon - |\delta|}{4\epsilon}\cos[(\bar{\omega}_L + \epsilon)\tau] + \frac{2\epsilon + |\delta|}{4\epsilon}\cos[(\bar{\omega}_L - \epsilon)\tau]\right\}e^{-(\gamma+k_{ab})\tau},\\
\langle F_{az}(\tau)F_{bz}(0)\rangle =& \mathrm{Var}(F_z)\frac{k_{ab}}{2\epsilon}\{\sin[(\bar{\omega}_L + \epsilon)\tau] - \sin[(\bar{\omega}_L - \epsilon)\tau]\}e^{-(\gamma+k_{ab})\tau}.
\end{aligned} \tag{A16}$$

Combining Eqs. (7), (8), and (A16), we obtain the correlation spectra of the two laser beams as

$$\tilde{g}_{aa}(\omega) = \frac{G^2 S_1^2 N_{\rm at}}{c^2}\left[\frac{2\epsilon+|\delta|}{\epsilon}\frac{\gamma+k_{ab}}{(\omega-\bar{\omega}_L-\epsilon)^2+(\gamma+k_{ab})^2}+\frac{2\epsilon-|\delta|}{\epsilon}\frac{\gamma+k_{ab}}{(\omega-\bar{\omega}_L+\epsilon)^2+(\gamma+k_{ab})^2}\right]+\frac{S_1}{2},$$

$$\tilde{g}_{bb}(\omega) = \frac{G^2 S_1^2 N_{\rm at}}{c^2}\left[\frac{2\epsilon-|\delta|}{\epsilon}\frac{\gamma+k_{ab}}{(\omega-\bar{\omega}_L-\epsilon)^2+(\gamma+k_{ab})^2}+\frac{2\epsilon+|\delta|}{\epsilon}\frac{\gamma+k_{ab}}{(\omega-\bar{\omega}_L+\epsilon)^2+(\gamma+k_{ab})^2}\right]+\frac{S_1}{2},$$

$$\tilde{g}_{ab}(\omega) = \frac{2G^2 S_1^2 N_{\rm at}}{c^2}\frac{k_{ab}}{\epsilon}\left[\frac{\bar{\omega}_L+\epsilon-\omega}{(\omega-\bar{\omega}_L-\epsilon)^2+(\gamma+k_{ab})^2}-\frac{\bar{\omega}_L-\epsilon-\omega}{(\omega-\bar{\omega}_L+\epsilon)^2+(\gamma+k_{ab})^2}\right]. \quad \text{(A17)}$$

3. Calculation of optical pumping rate

The total width of the optical transition is influenced by various factors, including Doppler broadening (approximately 500 MHz), natural linewidth (around 6 MHz), hyperfine splittings of the excited state (roughly 200 MHz), and Zeeman splittings of the ground state $F = 3$ level (about 100 kHz). We focus on the dominating Doppler broadening effect, which leads to an absorption cross section

$$\sigma_G(\Delta) = \pi r_e c f_1 g(\Delta_l), \quad \text{(A18)}$$

with

$$g(\Delta_l) = \frac{2\sqrt{2\ln 2/\pi}}{\Gamma_G}\exp\left(\frac{-4\ln 2}{\Gamma_G^2}\Delta_l^2\right) \quad \text{(A19)}$$

and

$$\Gamma_G = \frac{\bar{v}}{\lambda}\ln 2. \quad \text{(A20)}$$

Here, $r_e = 2.82\times10^{-15}$ m is the classical electron radius, $f_1 \approx 2/3$ is the D_2 transition's oscillator strength, and $\bar{v} = \sqrt{\frac{8k_B T_v}{\pi M}}$ is the thermal speed of the ^{85}Rb atoms, with $M = 1.42\times10^{-25}$ kg being the mass of a ^{85}Rb atom.

The width of the laser beam is several megahertz, significantly smaller than the laser detuning Δ_l. Therefore, we consider the laser beam to be a monochromatic beam. Consequently, the optical pumping rate can be expressed as

$$\gamma_{\rm op} = \Phi\sigma_G, \quad \text{(A21)}$$

where Φ is the number of photons per unit cross-sectional area per unit time. The cross-sectional area of the laser beam is about 10 mm^2, with a laser power of about 1 mW, establishing $\Phi = 3.84\times10^{15}$ s^{-1} m^{-2}. By combining Eqs. (A18)–(A21), the optical pumping rate for $\Delta_l = 1$ GHz is determined to be $\gamma_{\rm op} = 3.3$ s^{-1}.

4. Temperature calibration

The vapor cell is placed within a boron-nitride oven, which is heated by the ac current flow in twisted heating wires to avoid generating magnetic fields. The temperature of the oven is monitored by a thermocouple and stabilized to 0.1 K with an analog temperature controller. Heat is then transferred from the boron-nitride oven to the vapor cell, subsequently elevating the atomic vapor temperature. As a result of this indirect heating technique, the vapor temperature may not precisely match the oven's setting temperature. The heating system in our experiment closely resembles that of our prior study [23], and we observe a linear relationship between the vapor temperature and the setting temperature. Given the small temperature range in our experiments, we can establish an assumed relationship between the vapor temperature T_v and the setting temperature $T_{\rm set}$ as

$$T_v = a_T T_{\rm set} + T_0, \quad \text{(A22)}$$

where a_T and T_0 are constants.

We determine the vapor temperature T_v through the temperature-dependent spin-exchange effect of Rb atoms. The primary spin relaxation mechanisms within the OTS-coated cell comprise spin-exchange relaxation, wall relaxation, and optical pumping [17,22]. Consequently, the spin-relaxation rate γ can be represented as

$$\gamma \approx \gamma_{\rm se} + \gamma_w + \gamma_{\rm op}. \quad \text{(A23)}$$

Here, $\gamma_{\rm se} = q n_{\rm at}\sigma_{\rm se} v_{\rm rel}/2\pi$ represents the spin-exchange relaxation rate [47], where $q = \frac{2}{3}\frac{I(2I-1)}{(2I+1)^2} = \frac{5}{27}$ is the nuclear slowing-down factor for the $F = 3$ hyperfine level of ^{85}Rb atoms, $n_{\rm at} \approx \frac{1}{T_v}10^{14.178-4040/T_v}$ m^{-3} is the number density of the rubidium atoms, $\sigma_{\rm se} \approx 2\times10^{-14}$ cm^2 is the spin-exchange cross section [22], and $v_{\rm rel} \approx \sqrt{2}\bar{v}$ is the relative velocity between two rubidium colliding atoms. $\gamma_w = \frac{4N_b V_c}{S_c \bar{v}}$ denotes the wall-relaxation rate, where N_b is the number of coherent bounces between atoms and the cell wall, V_c is the cell volume, and S_c is the surface area of the cell. Therefore,

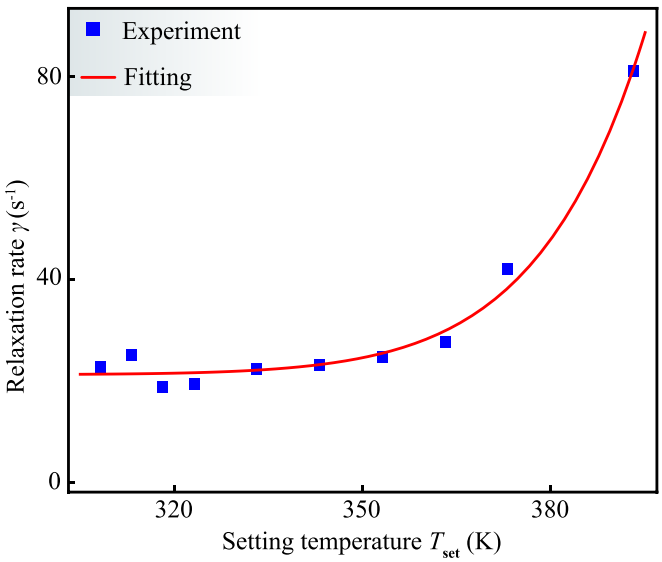

FIG. 6. Relaxation rate γ versus setting temperature $T_{\rm set}$. The fitting line is based on Eqs. (A22) and (A24).

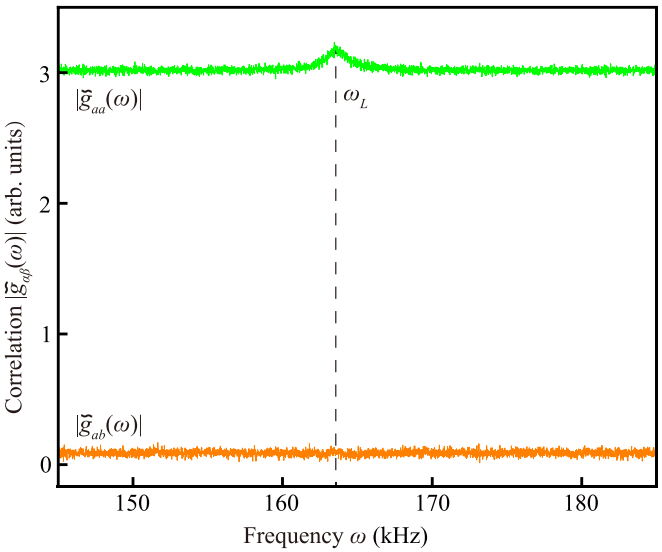

FIG. 7. Experimental auto- and cross-correlation spectra of the laser beams in the comparative experiment.

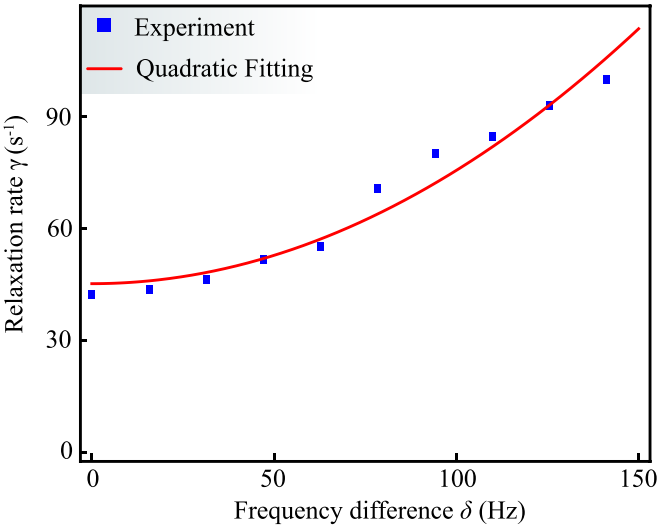

FIG. 8. Spin relaxation rate γ versus Larmor frequency difference δ at a vapor temperature of 342.0 K.

the relaxation rate γ can be further expressed as

$$\gamma = q n_{\rm at}(T_v)\sigma_{\rm se} v_{\rm rel}/2\pi + \gamma_w + \gamma_{\rm op}. \tag{A24}$$

Within our experimental parameters, the number-density magnitude $n_{\rm at}$ can vary over several orders, whereas the changes in $v_{\rm rel} \sim \sqrt{T_v}$, $\gamma_w \sim 1/\bar{v} \sim 1/\sqrt{T_v}$, and $\gamma_{\rm op} \sim \frac{e^{-1/T_v}}{\sqrt{T_v}}$ are comparatively smaller. Consequently, we can assume that $v_{\rm rel}$, $\gamma_{\rm op}$, and γ_w remain constant during vapor temperature adjustments. Based on Eqs. (A22) and (A24), the curve fitting of the relationship between γ and $T_{\rm set}$ in Fig. 6 reveals the correlation between the vapor temperature T_v and the set temperature $T_{\rm set}$ as

$$T_v = 0.87 T_{\rm set} + 18.89\ {\rm K}. \tag{A25}$$

Additionally, the fitting analysis reveals the wall-relaxation rate to be $\gamma_w = 17.9\ {\rm s}^{-1}$, closely aligning with findings from previous studies [22,37].

5. Correlation spectra in comparative experiment

The comparative experiment is conducted in a buffer-gas-filled cell, where the spin-noise signal is notably reduced compared to that in the OTS-coated cell due to pressure broadening induced by the buffer gas. Figure 7 shows the experimental auto- and cross-correlation spectra at a vapor temperature of 342.0 K. The autocorrelation spectrum $|\tilde{g}_{aa}(\omega)|$ exhibits an observable spin-noise peak at the Larmor frequency ω_L with a HWHM of 1.88 kHz, alongside a noise base. In both the OTS-coated cell and the buffer-gas-filled cell, the laser-beam powers are 1 mW, so the noise baseline is assumed to be the same. The amplitude ratio of the spin-noise signal to the noise baseline is approximately 0.05 in the buffer-gas-filled cell, while it is 3.07 in the OTS-coated cell, as depicted in Fig. 2(c). Using the noise baseline as a reference, we find that the spin-noise peak amplitude in the buffer-gas cell is approximately $1 - 0.05/3.07 = 98.4\%$ smaller than that in the OTS-coated cell. The cross-correlation spectrum $|\tilde{g}_{ab}(\omega)|$ displays nearly zero values, indicating a lack of synchronization between the two laser beams.

6. Relationship between spin relaxation and magnetic field gradient

The spin relaxation rate γ was observed to show a quadratic dependence on the magnetic-field inhomogeneity $\partial B/\partial y$ in a recent work [48], implying a quadratic relationship with the frequency difference $\delta = 466\,{\rm Hz/G} \times 5\,{\rm mm} \times \partial {\rm B}/\partial {\rm y}$. Therefore, we can assume

$$\gamma = a_y \delta^2 + \gamma_0, \tag{A26}$$

where a_y represents the coefficient characterizing the sensitivity of γ to δ and γ_0 denotes the baseline rate of spin relaxation unaffected by the magnetic field gradient. Figure 8 illustrates the experimental γ values for various δ values along with the quadratic curve fitting. Based on the fitting outcome, we derive

$$\gamma = 0.003\ {\rm Hz}^{-1}\delta^2 + 45.2\ {\rm s}^{-1}. \tag{A27}$$

[1] H. M. Oliveira and L. V. Melo, Sci. Rep. **5**, 11548 (2015).
[2] D. Zhang, Y. Cao, Q. Ouyang, and Y. Tu, Nat. Phys. **16**, 95 (2020).
[3] J. F. Totz, R. Snari, D. Yengi, M. R. Tinsley, H. Engel, and K. Showalter, Phys. Rev. E **92**, 022819 (2015).
[4] Z. F. Mainen and T. J. Sejnowski, Science **268**, 1503 (1995).

[5] R. Q. Quiroga, A. Kraskov, T. Kreuz, and P. Grassberger, Phys. Rev. E **65**, 041903 (2002).

[6] S. Roehr, P. Gulden, and M. Vossiek, in *2007 IEEE Radio and Wireless Symposium* (IEEE, Piscataway, NJ, 2007), pp. 551–554.

[7] S. Walter, A. Nunnenkamp, and C. Bruder, Phys. Rev. Lett. **112**, 094102 (2014).

[8] S.-B. Shim, M. Imboden, and P. Mohanty, Science **316**, 95 (2007).

[9] A. Pikovsky, M. Rosenblum, and J. Kurths, *Synchronization: A Universal Concept in Nonlinear Sciences*, Cambridge Nonlinear Science Series, Vol. 12 (Cambridge University Press, Cambridge, 2001).

[10] J.-N. Teramae and D. Tanaka, Phys. Rev. Lett. **93**, 204103 (2004).

[11] K. Yoshimura, J. Muramatsu, P. Davis, T. Harayama, H. Okumura, S. Morikatsu, H. Aida, and A. Uchida, Phys. Rev. Lett. **108**, 070602 (2012).

[12] S. Sunada, K. Arai, K. Yoshimura, and M. Adachi, Phys. Rev. Lett. **112**, 204101 (2014).

[13] F. Schmolke and E. Lutz, Phys. Rev. Lett. **129**, 250601 (2022).

[14] Y. Imai, S. Tsunegi, K. Nakajima, and T. Taniguchi, Phys. Rev. B **105**, 224407 (2022).

[15] E. B. Aleksandrov and V. Zapasskiĭ, Zh. Eksp. Teor. Fiz. **81**, 132 (1981) [Sov. Phys. JETP **54**, 64 (1981)].

[16] S. Crooker, D. Rickel, A. Balatsky, and D. Smith, Nature (London) **431**, 49 (2004).

[17] G. E. Katsoprinakis, A. T. Dellis, and I. K. Kominis, Phys. Rev. A **75**, 042502 (2007).

[18] G. E. Katsoprinakis, M. Polis, A. Tavernarakis, A. T. Dellis, and I. K. Kominis, Phys. Rev. A **77**, 054101 (2008).

[19] V. S. Zapasskii, A. Greilich, S. A. Crooker, Y. Li, G. G. Kozlov, D. R. Yakovlev, D. Reuter, A. D. Wieck, and M. Bayer, Phys. Rev. Lett. **110**, 176601 (2013).

[20] P. Glasenapp, N. A. Sinitsyn, L. Yang, D. G. Rickel, D. Roy, A. Greilich, M. Bayer, and S. A. Crooker, Phys. Rev. Lett. **113**, 156601 (2014).

[21] D. Roy, L. Yang, S. A. Crooker, and N. A. Sinitsyn, Sci. Rep. **5**, 9573 (2015).

[22] Y. Tang, Y. Wen, L. Cai, and K. Zhao, Phys. Rev. A **101**, 013821 (2020).

[23] S. Song, M. Jiang, Y. Qin, Y. Tong, W. Zhang, X. Qin, R.-B. Liu, and X. Peng, Phys. Rev. Appl. **17**, L011001 (2022).

[24] S. A. Crooker, J. Brandt, C. Sandfort, A. Greilich, D. R. Yakovlev, D. Reuter, A. D. Wieck, and M. Bayer, Phys. Rev. Lett. **104**, 036601 (2010).

[25] M. Oestreich, M. Römer, R. J. Haug, and D. Hägele, Phys. Rev. Lett. **95**, 216603 (2005).

[26] G. M. Müller, M. Römer, D. Schuh, W. Wegscheider, J. Hübner, and M. Oestreich, Phys. Rev. Lett. **101**, 206601 (2008).

[27] F. Li, Y. V. Pershin, V. A. Slipko, and N. A. Sinitsyn, Phys. Rev. Lett. **111**, 067201 (2013).

[28] N. A. Sinitsyn and Y. V. Pershin, Rep. Prog. Phys. **79**, 106501 (2016).

[29] H. Bao *et al.*, Nature (London) **581**, 159 (2020).

[30] L. Yang, P. Glasenapp, A. Greilich, D. Reuter, A. Wieck, D. Yakovlev, M. Bayer, and S. Crooker, Nat. Commun. **5**, 4949 (2014).

[31] K. Mouloudakis, G. Vasilakis, V. G. Lucivero, J. Kong, I. K. Kominis, and M. W. Mitchell, Phys. Rev. A **106**, 023112 (2022).

[32] K. Mouloudakis *et al.*, Phys. Rev. A **108**, 052822 (2023).

[33] V. G. Lucivero, N. D. McDonough, N. Dural, and M. V. Romalis, Phys. Rev. A **96**, 062702 (2017).

[34] R. Shaham, O. Katz, and O. Firstenberg, Phys. Rev. A **102**, 012822 (2020).

[35] W. Wang, M. Xia, W. Quan, and K. Wei, Quantum Sci. Technol. **9**, 035048 (2024).

[36] The cell contains a mixture of ^{85}Rb and ^{87}Rb in natural abundance, but under our experimental conditions, the contribution from ^{87}Rb is negligibly small.

[37] G. Zhang, L. Wei, M. Wang, and K. Zhao, J. Appl. Phys. **117**, 043106 (2015).

[38] C. W. Gardiner *et al.*, *Handbook of Stochastic Methods* (Springer, Berlin, 1985), Vol. 3.

[39] A. Z. Goldberg, P. De La Hoz, G. Björk, A. B. Klimov, M. Grassl, G. Leuchs, and L. L. Sánchez-Soto, Adv. Opt. Photonics **13**, 1 (2021).

[40] D. Suter and J. Mlynek, in *Advances in Magnetic and Optical Resonance*, edited by W. S. Warren (Academic Press, San Diego, CA, 1991), Vol. 16, pp. 1–83.

[41] K. Hammerer, A. S. Sørensen, and E. S. Polzik, Rev. Mod. Phys. **82**, 1041 (2010).

[42] W. Cao, X. Lu, X. Meng, J. Sun, H. Shen, and Y. Xiao, Phys. Rev. Lett. **124**, 030401 (2020).

[43] C. Alcock, V. Itkin, and M. Horrigan, Can. Metall. Q. **23**, 309 (1984).

[44] U. M. Maurer, IEEE Trans. Inf. Theory **39**, 733 (1993).

[45] P. Peng, W. Cao, C. Shen, W. Qu, J. Wen, L. Jiang, and Y. Xiao, Nat. Phys. **12**, 1139 (2016).

[46] J. Kong, R. Jiménez-Martínez, C. Troullinou, V. G. Lucivero, G. Tóth, and M. W. Mitchell, Nat. Commun. **11**, 1 (2020).

[47] A. T. Dellis, M. Loulakis, and I. K. Kominis, Phys. Rev. A **90**, 032705 (2014).

[48] S. Pustelny, D. F. Jackson Kimball, S. M. Rochester, V. V. Yashchuk, and D. Budker, Phys. Rev. A **74**, 063406 (2006).